

Gravity waves and high-altitude CO₂ ice cloud formation in the Martian atmosphere

Erdal Yiğit,^{1,2} Alexander S. Medvedev,^{2,3} Paul Hartogh²

Corresponding author: E. Yiğit, Space Weather Group, School of Physics Astronomy and Computational Sciences, MSN:3F3, Fairfax, VA 22030, USA. (eyigit@gmu.edu)

¹School of Physics, Astronomy, and Computational Sciences, George Mason University, Fairfax, Virginia, USA.

²Max Planck Institute for Solar System Research, Göttingen, Germany.

³Institute of Astrophysics, Georg-August University, Göttingen, Germany.

arXiv:1505.04472v1 [astro-ph.EP] 17 May 2015

We present the first general circulation model simulations that quantify and reproduce patches of extremely cold air required for CO₂ condensation and cloud formation in the Martian mesosphere. They are created by subgrid-scale gravity waves (GWs) accounted for in the model with the interactively implemented spectral parameterization. Distributions of GW-induced temperature fluctuations and occurrences of supersaturation conditions are in a good agreement with observations of high-altitude CO₂ ice clouds. Our study confirms the key role of GWs in facilitating CO₂ cloud formation, discusses their tidal modulation, and predicts clouds at altitudes higher than have been observed to date.

1. Introduction

Carbon dioxide ice clouds have been numerous and unambiguously detected in the middle atmosphere (50–100 km) of Mars [e.g., *Schofield et al.*, 1997; *Clancy and Sandor*, 1998; *Clancy et al.*, 2007; *Montmessin et al.*, 2007; *McConnochie et al.*, 2010; *Vincendon et al.*, 2011]. The most recent and detailed references to observations and climatology of these clouds are given in the works by *Sefton-Nash et al.* [2013, Figures 6 to 9 for distribution over latitude, longitude, L_s and altitude] and *Listowski et al.* [2014, Table 1 for general characteristics of detected mesospheric clouds, and references therein]. Observations show that, in average, temperatures in the Martian mesosphere are not cold enough to sustain CO₂ condensation. *Clancy and Sandor* [1998] speculated that CO₂ ice forms in patches of cold air created occasionally by temperature fluctuations associated with tides and gravity waves (GWs). This hypothesis has been further supported by numerical simulations of *Spiga et al.* [2012]. Using a mesoscale (GW-resolving) Martian meteorological model, they demonstrated that GWs generated in the troposphere have amplitudes in the mesosphere sufficient to form pockets of cold air with temperatures below the CO₂ condensation threshold. On the other hand, Martian general circulation models (MGCMs) turned out to be less successful in reproducing cold temperatures required for the formation of mesospheric CO₂ ice clouds. Thus, *González-Galindo et al.* [2011] reported that mesopause temperatures simulated with the Laboratoire de Météorologie Dynamique (LMD) MGCM tended to be low near the equator at $L_s < 150^\circ$ and in middle latitudes afterwards, where high-altitude clouds are usually observed, albeit always remained few Kelvin degrees above the condensation point. Similarly, temperatures simulated with the

Max Planck Institute (MPI) MGCM never dropped below that of CO₂ condensation [e.g., *Medvedev et al.*, 2013, Figure 1].

A possible reason for MGCM failures to reproduce CO₂ ice cloud formation in the mesosphere is that mesoscale GWs (with horizontal scales from tens to few hundred km) are mostly unresolved by such models. Since dynamical and thermal effects of GWs in the middle and upper atmosphere are significant and cannot be neglected, they have to be parameterized in GCMs [see the review of *Yiğit and Medvedev*, 2015, on the recent progress with relevant studies in the Earth atmosphere]. On Mars, GW sources are stronger than on Earth, and significant wave-induced dynamical [*Medvedev et al.*, 2011a] and thermal [*Medvedev and Yiğit*, 2012] effects are being increasingly revealed. In particular, the simulations of *Medvedev and Yiğit* [2012] with the MPI–MGCM have demonstrated for the first time that accounting for the GW-induced cooling rates helped to reproduce the cold mesospheric temperatures retrieved from Mars Odyssey aerobraking measurements.

In addition to the ability of parameterizations to account for acceleration/deceleration of the mean flow and mean heating/rates due to subgrid-scale GWs, they provide amplitudes of GW-induced temperature fluctuations. In this paper, we extend the study of *Spiga et al.* [2012] from demonstrating a potential role of GWs in creating pockets of sub-condensation temperatures to explicitly quantifying and capturing these processes in Martian GCMs, which open new perspectives of modeling CO₂ ice cloud formation. For that, we employ the MPI–MGCM with the implemented subgrid-scale GW parameterization of *Yiğit et al.* [2008]. The model and GW scheme are described in Section 2. The simulated global distributions of GW activity and pockets of air with subcondensation temperatures are

presented in Section 3. Their geographical distributions, and local and universal time variations are discussed in Sections 4 and 5, correspondingly.

2. Martian General Circulation Model and Gravity Wave Scheme

The Max Planck Institute Martian General Circulation Model (MPI-MGCM) is a first principle three-dimensional spectral model extending from the surface to the lower thermosphere (3.6×10^{-6} hPa, ~ 150 -160 km). The current simulations have been performed with 67 hybrid levels, and T21 horizontal resolution (64 and 32 grid points in longitude and latitude, correspondingly). The model has a complete set of physical parameterizations suitable for Mars, which have been described in detail in the works by *Hartogh et al.* [2005, 2007]; *Medvedev and Hartogh* [2007], and *Medvedev et al.* [2011b]. In the mesosphere and thermosphere, in the region of particular interest for CO₂ cloud formation, heating/cooling effects due to radiative transfer in gaseous CO₂ are taken into account with the exact non-LTE ALI-ARMS code of *Kutepov et al.* [1998] and *Gusev and Kutepov* [2003] optimized with respect to a number of vibrational levels.

The extended nonlinear spectral GW parameterization is described in detail in the work by *Yiğit et al.* [2008], and its implementation and application in the MPI-MGCM is given in the paper by *Medvedev et al.* [2011b]. The scheme is appropriate for planetary whole atmosphere models extending into the thermosphere. It has been extensively tested and used for studying GW-induced vertical coupling processes in Earth's atmosphere [*Yiğit et al.*, 2009, 2012, 2014; *Yiğit and Medvedev*, 2009, 2010]. The scheme calculates vertical propagation of subgrid-scale harmonics systematically accounting for the major wave dissipation mechanisms in the Martian atmosphere: due to nonlinear breaking/saturation,

molecular viscosity and thermal conduction. An empirical distribution of GW spectrum is specified at the source level in the lower atmosphere, and the scheme calculates at consecutive vertical levels the momentum and temperature tendencies imposed by GWs on the larger-scale (resolved) atmospheric flow. In this study, we use the same GW source specification as in the previous works [Medvedev and Yiğit, 2012; Medvedev et al., 2013]. Namely, the horizontally uniform and temporally constant amplitude of GW velocity fluctuations ($\sim 1 \text{ m s}^{-1}$) was prescribed at the source level ($p = 260 \text{ Pa}$), harmonics were launched along and against the direction of the local wind, and a Gaussian spectrum over horizontal phase speeds was assumed.

The model was run for 40 sols, approximately corresponding to $L_s = 0 - 20^\circ$, that is, for a Northern Hemisphere spring equinox. The low dust optical depth ($\tau = 0.2$ in visible) appropriate for this season, and the low solar flux of $F_{10.7} = 80 \times 10^{-22} \text{ W m}^{-2} \text{ Hz}^{-1}$ have been kept constant throughout the simulations. Model mean fields to be shown have been calculated as 60-sol averaged, and the universal time plots are based on hourly outputs.

3. Gravity Wave Activity and Subsaturation Temperatures

The GW parameterization calculates vertical profiles $|u'_j(z)|$ of amplitudes of horizontal velocity fluctuations for each wave harmonic j of the GW spectrum. The contributions of all harmonics yield the root-mean-square (RMS) $\sigma_u(z) = \sqrt{\sum_j |u'_j(z)|^2} \equiv |u'|$, which describes the net GW-induced variance of horizontal velocity. Because the kinetic (E_k) and mechanical potential (E_p) energies are equal for GW harmonics under consideration [Geller and Gong, 2010],

$$E_k = \frac{1}{2}|u'|^2 = \frac{1}{2}\left(\frac{g}{N}\right)^2 \frac{|T'|^2}{T^2} = E_p, \quad (1)$$

where g is the acceleration of gravity, N is the Brunt-Väisälä frequency, and T is the mean (resolved by the GCM) neutral temperature, the total wave-induced RMS temperature perturbations $|T'|$ can be computed from $|u'|$. Note that $|T'|$ provides no information about phases of contributing harmonics. Unlike with wave-resolving simulations, $|T'(z)|$ does not describe instantaneous wave fields, but only characterizes the magnitude of the parameterized subgrid-scale GWs. Individual wave-induced temperature fluctuations in each point are, thus, bound by $|T'|$: $-|T'| \leq T' \leq |T'|$.

The simulated temperature T (black contours) and GW activity $|T'|$ (color shades) are plotted in Figure 1a in the form of zonally and temporally averaged pressure-latitude cross-sections. The GW activity varies appreciably both with height and latitude. Temperature fluctuations increase with altitude from about 2 K near the source in the troposphere (at 260 Pa), peak near the mesopause (~ 105 km) with $|T'| \sim 12$ K around low-latitudes, and reach 20 K in the polar regions in both hemispheres. Enhanced GW activity in the mesopause regions occurs as a result of exponential amplitude growth due the density decay, and the attenuation of upward propagating lower atmospheric GWs by nonlinear diffusion and increasing molecular viscosity. Selective filtering of GW harmonics by the winds is also at play, and is mainly responsible for the latitudinal distribution of $|T'|$.

CO₂ condensation requires a temperature drop below the saturation level, which is calculated in our model with the Clausius-Clayperon relation as the function of pressure. Our GCM does not include a detailed cloud microphysics. Instead, the process of ice particle nucleation is accounted for by a significant degree of supersaturation: CO₂ ice is considered to be formed at pressures 1.35 times larger than that from the Clausius-

Clayperon relation, as suggested by *Glandorf et al.* [2002] and utilized by *Kuroda et al.* [2013]. As already mentioned, temperature T in our simulations never fell below thus defined saturation level T_s , which can also be seen in Figure 1a. However, taking excursions around the resolved temperature induced by parameterized small-scale GWs into account can yield the necessary CO₂ ice condensation conditions. Having no way of knowing individual wave profiles, one nevertheless can argue that condensation may occur only when $T - |T'| \leq T_s$. We count these events at every time step over the course of model integration, and their number (divided by the total number of time steps) defines the probability P of CO₂ ice cloud formation over the time period. Alternatively, the value of P shows the percentage of time when super-saturation conditions exist.

Figure 1b presents thus calculated P in percentage (shaded), and the geopotential height in km is overplotted with contours for more convenient visualization of geographical altitudes. It is seen that chances of encountering CO₂ super-saturation conditions increase rapidly with height from the upper mesosphere upward. Visual inspection of panels a and b reveals that there is a remarkable correlation between the GW-induced temperature perturbations and the chances of CO₂ clouds to form. The largest probabilities are around the mesopause (P up to 10% at low-latitudes and exceed 20% at high-latitudes). More pockets of cold air with subcondensation temperatures in these regions are due to the combined effect of globally lowest temperatures and largest GW perturbations. In the upper mesosphere P is up to 5% around the equator. It approximately matches the region where the CO₂ clouds have been observed over this season [e.g., *Sefton-Nash et al.*, 2013, and references therein], while capturing the fact that the cloud events are relatively

rare. If subgrid-scale GW effects are not included in simulations, the supersaturation of CO₂ does not occur at all, that is, $P = 0$ globally (not shown).

These results indicate that (1) if subgrid-scale GW effects are included, then the supersaturation condition is fulfilled globally in up to $> 20\%$ of the time in the mesosphere and mesopause region over a large range of altitudes and latitudes; (2) regions of most probable cloud formation coincide with the places of enhanced GW activity. A note of caution should be added here. Due to the parameterized nature of GWs in our simulations, the occurrences of clouds are not deterministic. Probability P quantifies regions where CO₂ condensation is most likely, but individual temperature profiles may not yield temperatures below T_s due to particular phases of the harmonics and their interference.

4. Mean Geographical Distribution

We next investigate the geographical details of the modeled link between the GW-induced temperature fluctuations $|T'|$ and the probability of CO₂ ice cloud formation P . Figure 2 presents the mean latitude-longitude cross-sections of $|T'|$ (upper panels) and P (lower panels) at two representative pressure levels in the upper mesosphere and around the mesopause, $p = 10^{-3}$ Pa (left) and 10^{-4} Pa (right), respectively. Major topographic features are indicated in the lower panels with blue-to-red (that is, low-to-high levels) contour scales.

There is a significant amount of spatial variability in the distribution of $|T'|$ at both altitudes, in particular, around the mesopause. In the mesosphere, GW-induced temperature variations can reach 4–12 K, while higher up around the mesopause, $|T'|$ is up to > 20 K. Distributions of cloud formation probability P show also a marked spatial vari-

ability with larger values concentrated mainly around the high-latitudes and the equator in the mesosphere with peak values of $P \sim 2 - 3\%$ around 60°W–120°W, and $P \sim 14\%$ around 60°E–160°E. These regions partially coincide with those where clouds have been observed more often [Spiga *et al.*, 2012, Figure 2]. There is an appreciable probability of cloud formation around the mesopause region. Very large values of P are seen, in particular, at low-latitudes and near both poles with values exceeding 24% locally. Overall, the results indicate that there exists a very good geographical correlation between the GW activity, and the chances of mesospheric CO₂ ice clouds to form, especially, near the mesopause. Locations of such spots of high wave activity (and cloud formation as well) are not clearly linked down to surface features. This is because the GW parameterization accounts for “non-orographic” waves, which propagate to the mesosphere and lower thermosphere more favorably than their topographically forced counterparts with very slow observed phase speeds. The regions of enhanced $|T'|$ are apparently the results of modulation of GW propagation by larger-scale meteorological features in the underlying layers, by quasi-stationary waves, for instance.

5. Local Time and Universal Time Variations

The majority of observations of mesospheric CO₂ ice clouds have been performed from spacecraft inserted on polar orbits (Mars Global Surveyor, Mars Express, Mars Odyssey, Mars Reconnaissance Orbiter). This means that the measurements were always taken at narrow intervals of local times, mainly on a day side of the planet. To investigate how this may bias the cloud statistics, we plotted the simulated distributions at certain local day- and night-times, as if they were observed from such an orbiter. Figure 3 presents

the latitude-longitude distributions of the GW-induced temperature perturbations $|T'|$ (contours) and probability of CO₂ supersaturation P (blue shadings) at 0200 LT (left) and 1400 LT (right) in the mesopause region at $p = 0.0001$ Pa, where the coldest mean temperatures and largest GW-induced temperature fluctuations coexist.

It is immediately seen that more clouds have chances to form at night-times. Because most of cloud observations took place on the day-side of the orbits, our results may serve as an indication that the amount of such clouds on Mars is underestimated. Magnitudes of GW activity $|T'|$ are approximately equal throughout all local times, however mean temperatures T vary significantly. With colder night-side T , the supersaturation condition $T - |T'| \leq T_s$ occurs more often, while local enhancements of $|T'|$ and P still substantially correlate.

Further insight into how subgrid-scale GWs mediate CO₂ ice cloud formation can be gained from Figure 4. It shows universal time variations of the simulated wave activity $|T'|$ and probability of condensation P . The left panel presents the Hovmöller diagram (longitude vs time) for these quantities where they are the largest in our simulations: over the equator at around the mesopause level ($p = 0.0001$ Pa). It demonstrates that cloud occurrences are extremely localized in space and time, and may appear as almost random. However, westward propagating variations of P with clear migrating diurnal and semidiurnal tide signatures can be seen. Regions of high wave activity are also modulated by the diurnal and semidiurnal solar tides. Although there is a strong correlation between $|T'|$ and P , not all maxima of GW activity are accompanied by CO₂ condensation conditions. The right panel displays this with the height-universal time cross-sections.

Tides affect GW propagation mainly by altering zonal winds. Therefore, maxima of GW activity (contours) are phase-shifted with respect to peaks of tidally modulated temperature T . Condensation occurs only when and where T and $|T'|$ appropriately match the saturation condition (shaded areas). Thus, our simulations provide further illustration for the hypothesis of *Clancy and Sandor* [1998] regarding the combined role of tides and GWs in mesospheric CO₂ cloud formation.

6. Conclusions

We presented the first simulations with a general circulation model of distributions of localized patches of air at temperatures below the CO₂ condensation threshold. They have been performed with the Max Planck Institute Martian General Circulation Model (MGCM) with the implemented subgrid-scale gravity wave (GW) parameterization of *Yiğit et al.* [2008]. The main conclusions are the following.

- GWs facilitate cloud formation by creating pockets of cold air with temperatures below that required for CO₂ condensation. Without GWs, high-altitude cloud formation is impossible, at least in our simulations.
- The simulated occurrences of supersaturated temperatures are in a good agreement with observations of CO₂ clouds in the mesosphere.
- The approach with utilizing parameterized GWs can be used for quantifying the mechanism of mesospheric CO₂ cloud formation, and reproducing it in MGCMs.
- Our study predicts more clouds than observed at higher altitudes, and in polar regions.

The last prediction requires a discussion, which we have left to this point. Why the even-higher-altitude CO₂ clouds have not been observed to date? One possibility is that they cannot form for microphysical reasons due to an insufficient amount of nucleation particles, etc. This can be explored by implementing a state-of-the-art microphysics scheme, and using the approach described in this paper. The second possibility is that such clouds are too thin, sizes of ice particles are too small, and the existing instrumentation was simply unable to detect them. Finally, our prediction can be altered when more observations become available to constrain gravity wave sources in the lower atmosphere and atomic oxygen that determines CO₂ IR cooling in the mesosphere [Medvedev *et al.*, 2015]. This prediction provides a testbed for assessing our understanding of the Martian middle atmosphere physics.

Acknowledgments. Data supporting the figures are available from EY (eyigit@gmu.edu). EY was partially funded by NASA grant NNX13AO36G. The work was partially supported by German Science Foundation (DFG) grant ME2752/3-1.

References

- Clancy, R. T., and B. J. Sandor (1998), CO₂ ice clouds in the upper atmosphere of Mars, *Geophys. Res. Lett.*, 25(4), 489–492.
- Clancy, R. T., M. J. Wolff, B. A. Whitney, B. A. Cantor, and M. D. Smith (2007), Mars equatorial mesospheric clouds: Global occurrence and physical properties from Mars Global Surveyor Thermal Emission Spectrometer and Mars Orbiter Camera limb observations, *J. Geophys. Res.*, 112(E4), doi:10.1029/2006JE002805.

- Geller, M. A., and L. Gong (2010), Gravity wave kinetic, potential, and vertical fluctuation energies as indicators of different frequency gravity waves, *J. Geophys. Res.*, *115*, D1111, doi:10.1029/2009JD012266.
- Glandorf, D. L., A. Colaprete, M. A. Tolbert, and O. B. Toon (2002), C₂ snow on Mars and early Earth: Experimental constraints, *Icarus*, *160*, 66–72.
- González-Galindo, F., A. Määttänen, F. Forget, and A. Spiga (2011), The martian mesosphere as revealed by CO₂ cloud observations and general circulation modeling, *Icarus*, *216*, 10–22, doi:10.1016/j.icarus.2011.08.006.
- Gusev, O. A., and A. A. Kutepov (2003), Non-lte gas in planetary atmospheres, in *Stellar Atmosphere Modeling, ASP Conference Series*, vol. 288, edited by I. Hubeny, D. Mihalas, and K. Werner, pp. 318–330, Springer.
- Hartogh, P., A. S. Medvedev, T. Kuroda, R. Saito, G. Villanueva, A. G. Feofilov, A. A. Kutepov, and U. Berger (2005), Description and climatology of a new general circulation model of the Martian atmosphere, *J. Geophys. Res.*, *110*, E11008, doi:10.1029/2005JE002498.
- Hartogh, P., A. S. Medvedev, and C. Jarchow (2007), Middle atmosphere polar warmings on mars: simulations and study on the validation with sub-millimeter observations, *Planet. Space Sci.*, *55*, 1103–1112.
- Kuroda, T., A. S. Medvedev, Y. Kasaba, and P. Hartogh (2013), Carbon dioxide ice clouds, snowfalls, and baroclinic waves in the northern winter polar atmosphere of mars, *Geophys. Res. Lett.*, *40*, doi:10.1002/grl.50326.

- Kutepov, A. A., O. A. Gusev, and V. P. Ogibalov (1998), Solution of the non-lte problem for molecular gas in planetary atmospheres: Superiority of accelerated lambda iteration, *J. Quant. Spectrosc. Radiat. Transfer*, *60*, 199–220.
- Listowski, C., A. Määttänen, F. Montmessin, A. Spiga, and F. Lefèvre (2014), Modeling the microphysics of CO₂ ice clouds within wave-induced cold pockets in the martian mesosphere, *Icarus*, *237*, 239–261, doi:10.1016/j.icarus.2014.04.022.
- McConnochie, T., J. B. III, D. Savransky, M. Wolff, A. Toigo, H. Wang, M. Richardson, and P. Christensen (2010), Themis-vis observations of clouds in the martian mesosphere: Altitudes, wind speeds, and decameter-scale morphology, *Icarus*, *210*(2), 545 – 565, doi:10.1016/j.icarus.2010.07.021.
- Medvedev, A. S., and P. Hartogh (2007), Winter polar warmings and the meridional transport on Mars simulated with a general circulation model, *Icarus*, *186*, 97–110.
- Medvedev, A. S., and E. Yiğit (2012), Thermal effects of internal gravity waves in the Martian upper atmosphere, *Geophys. Res. Lett.*, *39*, L05201, doi:10.1029/2012GL050852.
- Medvedev, A. S., E. Yiğit, and P. Hartogh (2011a), Estimates of gravity wave drag on Mars: indication of a possible lower thermosphere wind reversal, *Icarus*, *211*, 909–912, doi:10.1016/j.icarus.2010.10.013.
- Medvedev, A. S., E. Yiğit, P. Hartogh, and E. Becker (2011b), Influence of gravity waves on the Martian atmosphere: General circulation modeling, *J. Geophys. Res.*, *116*, E10004, doi:10.1029/2011JE003848.
- Medvedev, A. S., E. Yiğit, T. Kuroda, and P. Hartogh (2013), General circulation modeling of the martian upper atmosphere during global dust storms, *J. Geophys. Res.*, *118*,

1–13, doi:10.1002/jgre.20163, 2013.

Medvedev, A. S., F. González-Galindo, E. Yiğit, A. G. Feofilov, F. Forget, and P. Hartogh (2015), Cooling of the Martian thermosphere by CO₂ radiation and gravity waves: An intercomparison study with two general circulation models, *J. Geophys. Res. Planets*, *120*, doi:10.1002/2015JE004802.

Montmessin, F., B. Gondet, J.-P. Bibring, Y. Langevin, P. Drossart, F. Forget, and T. Fouchet (2007), Hyperspectral imaging of convective CO₂ ice clouds in the equatorial mesosphere of mars, *J. Geophys. Res. Planets*, *112*(E11), doi:10.1029/2007JE002944.

Schofield, J. T., J. R. Barnes, D. Crisp, R. M. Haberle, S. Larsen, J. A. Magalhes, J. R. Murphy, A. Seiff, and G. Wilson (1997), The Mars Pathfinder atmospheric structure investigation/meteorology (ASI/MET) experiment, *Science*, *278*(5344), 1752–1758, doi:10.1126/science.278.5344.1752.

Sefton-Nash, E., N. A. Teanby, L. Montabone, P. G. J. Irwin, J. Hurley, and S. B. Calcutt (2013), Climatology and first-order composition estimates of mesospheric clouds from mars climate sounder limb spectra, *Icarus*, *222*, 342–356, doi:10.1016/j.icarus.2012.11.012.

Spiga, A., F. González-Galindo, M.-A. Lopez-Valverde, and F. Forget (2012), Gravity waves, cold pockets and CO₂ clouds in the martian mesosphere, *Geophys. Res. Lett.*, *39*, L02201, doi:10.1029/2011GL050343.

Vincendon, M., C. Pilorget, B. Gondet, S. Murchie, and J.-P. Bibring (2011), New near-IR observations of mesospheric CO₂ and H₂O clouds on Mars, *J. Geophys. Res. Planets*, *116*(E11), doi:10.1029/2011JE003827.

- Yiğit, E., and A. S. Medvedev (2009), Heating and cooling of the thermosphere by internal gravity waves, *Geophys. Res. Lett.*, *36*, L14807, doi:10.1029/2009GL038507.
- Yiğit, E., and A. S. Medvedev (2010), Internal gravity waves in the thermosphere during low and high solar activity: Simulation study., *J. Geophys. Res.*, *115*, A00G02, doi:10.1029/2009JA015106.
- Yiğit, E., and A. S. Medvedev (2015), Internal wave coupling processes in Earth's atmosphere, *Adv. Space Res.*, *55*, 983–1003, doi:10.1016/j.asr.2014.11.020.
- Yiğit, E., A. D. Aylward, and A. S. Medvedev (2008), Parameterization of the effects of vertically propagating gravity waves for thermosphere general circulation models: Sensitivity study, *J. Geophys. Res.*, *113*, D19106, doi:10.1029/2008JD010135.
- Yiğit, E., A. S. Medvedev, A. D. Aylward, P. Hartogh, and M. J. Harris (2009), Modeling the effects of gravity wave momentum deposition on the general circulation above the turbopause, *J. Geophys. Res.*, *114*, D07101, doi:10.1029/2008JD011132.
- Yiğit, E., A. S. Medvedev, A. D. Aylward, A. J. Ridley, M. J. Harris, M. B. Moldwin, and P. Hartogh (2012), Dynamical effects of internal gravity waves in the equinoctial thermosphere, *J. Atmos. Sol.-Terr. Phys.*, *90–91*, 104–116, doi:10.1016/j.jastp.2011.11.014.
- Yiğit, E., A. S. Medvedev, S. L. England, and T. J. Immel (2014), Simulated variability of the high-latitude thermosphere induced by small-scale gravity waves during a sudden stratospheric warming, *J. Geophys. Res. Space Physics*, *119*, doi:10.1002/2013JA019283.

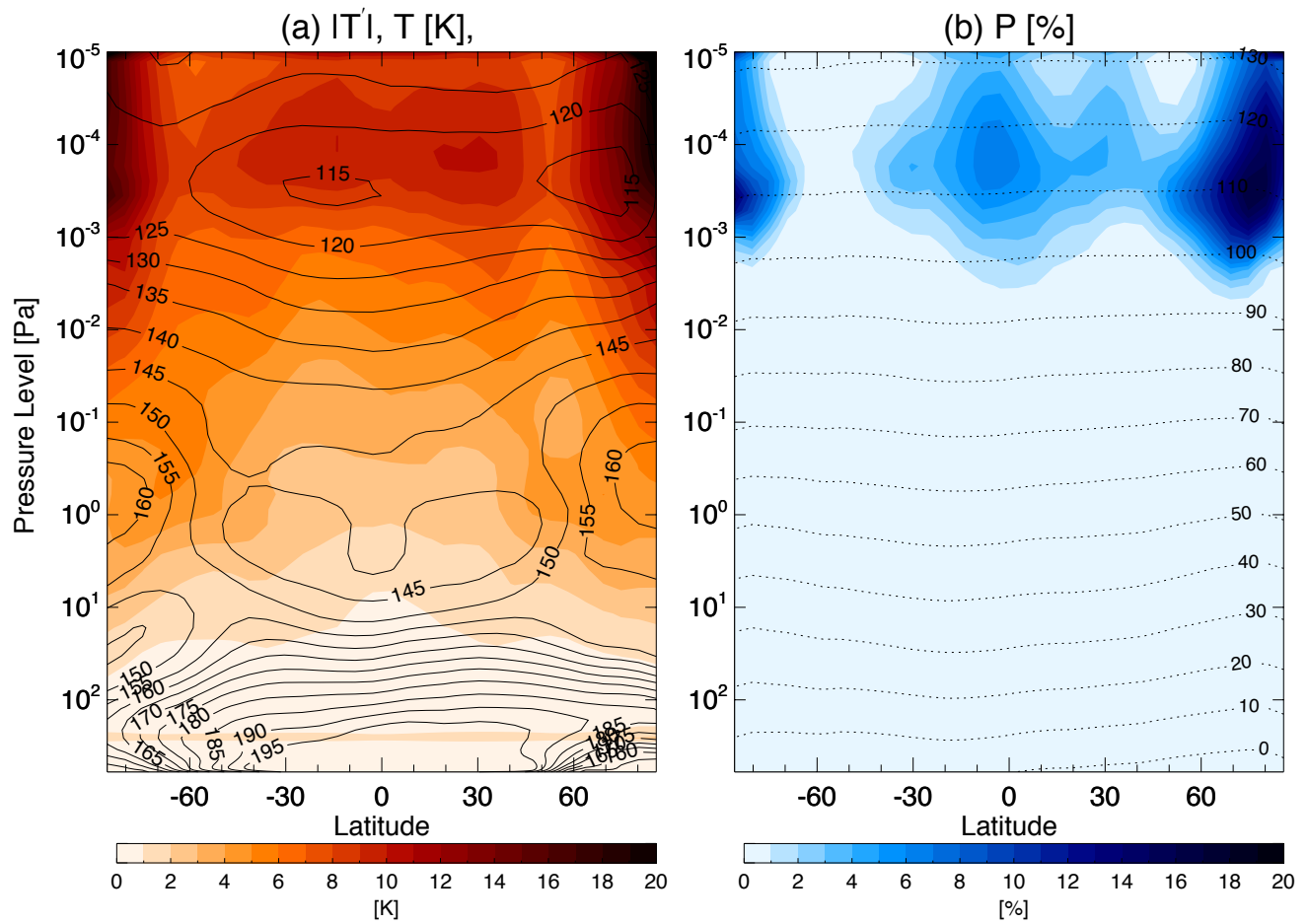


Figure 1. Mean (40-sol) (a) zonal mean neutral temperature T (contour lines) and gravity wave-induced temperature perturbation $|T'|$ (color shaded) in Kelvin degrees; (b) probability P of CO₂ ice cloud formation in percentage (blue shaded), and the geopotential height of the corresponding pressure levels in km (contours).

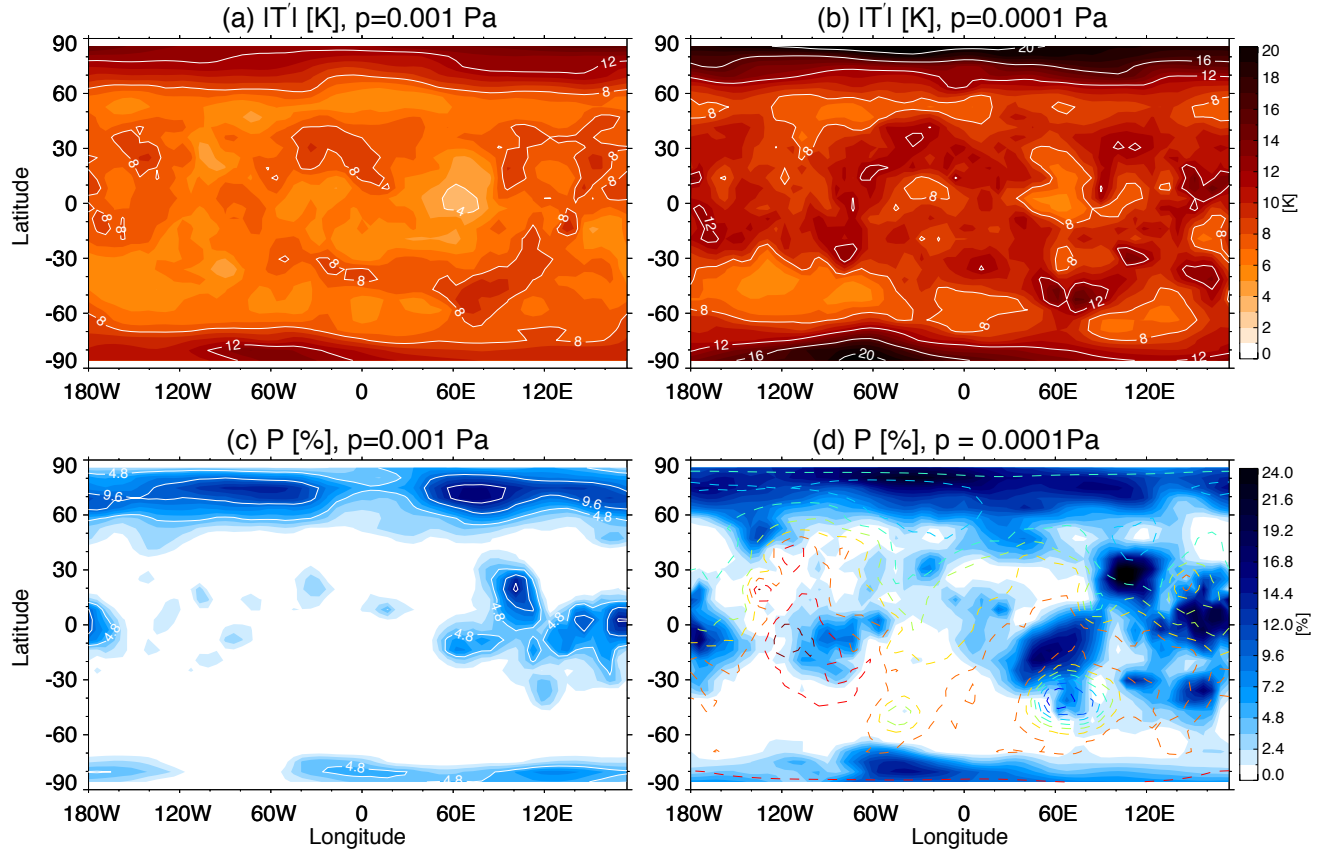


Figure 2. Geographical distribution of the mean gravity wave-induced temperature perturbations $|T'|$ in K (upper panels) and the probability of CO₂ ice cloud formation P in percentage (lower panels) at 10^{-3} (left) and 10^{-4} Pa (right). Dashed lines in the lower panels show the main topographical features from low (blue) to high levels (red).

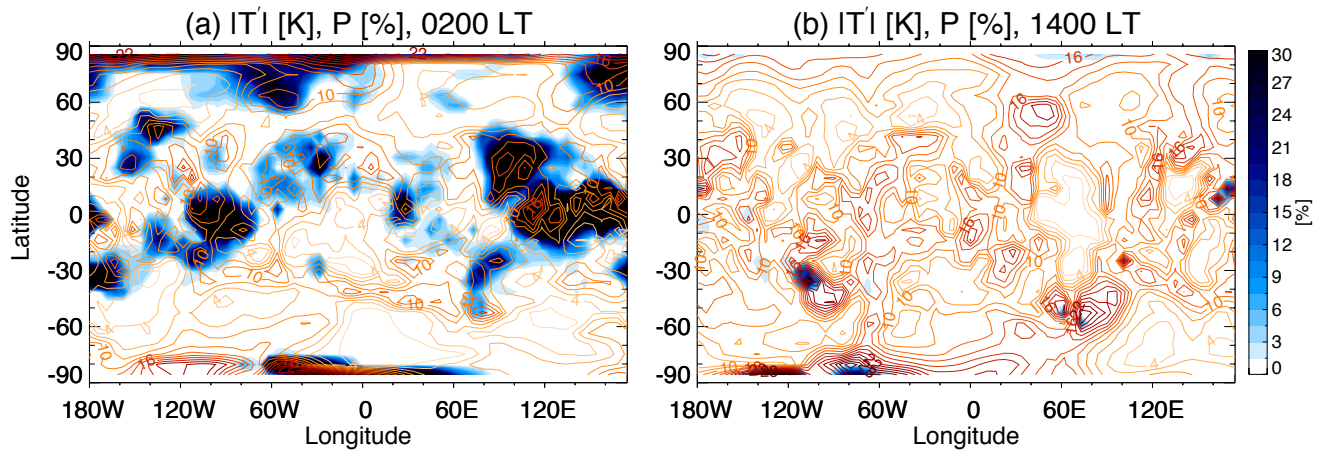


Figure 3. Latitude-longitude cross-sections of the simulated GW-induced temperature fluctuations (contours), and the probability P of CO₂ supersaturation (blue shaded) around the mesopause ($p=0.0001$ Pa) during a) local night (0200 LT), and b) local afternoon (1400 LT). Contour intervals are 3 K.

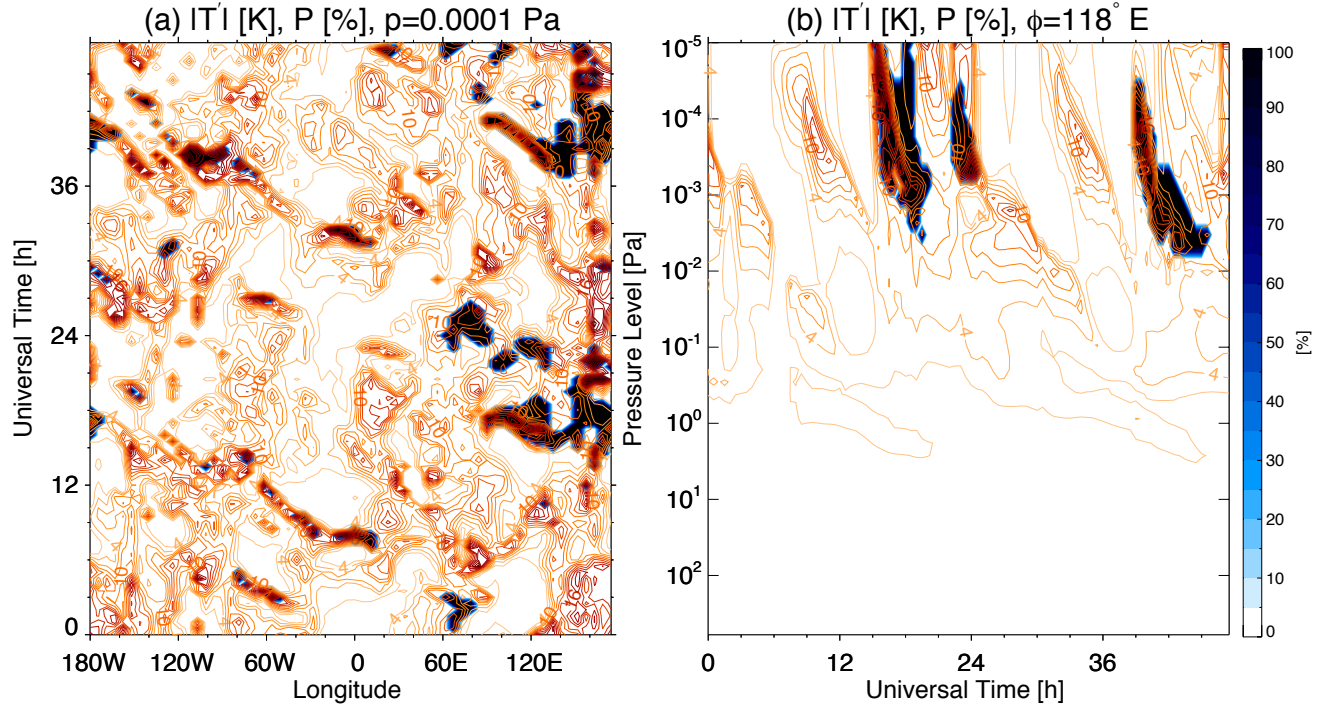


Figure 4. Temporal variations (over 48-hour period) of the modeled GW-induced temperature perturbations (contours), and the probability of CO₂ ice cloud formation (blue shading) close to the equator ($\theta = 2.7^\circ\text{N}$): (a) Universal time (UT)-longitude distributions; (b) pressure level (in Pa) - UT distributions at 118°E .